Paleomagnetism and Investigation of 40 Ma Lavas, Liverpool Range, New South Wales, Australia

Senior Project

For The Physics Department

Cal Poly State University, San Luis Obispo

This Project Completes

Required Coursework for the Degree

Bachelors of Science in Physics

By Nathan M. Padilla

June 2011

Table of Contents

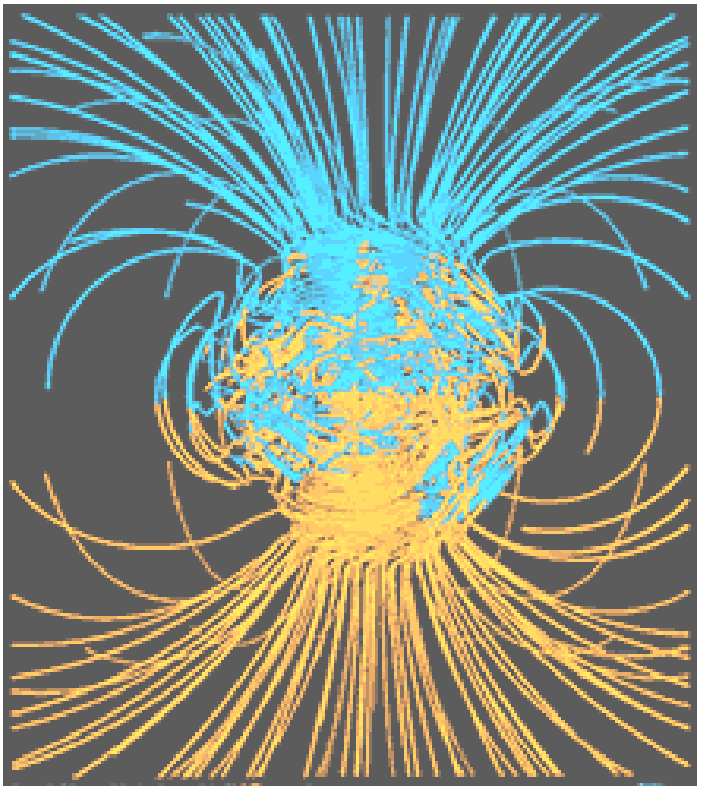

Figure 1: Computer simulated (reversed) magnetic field lines of the earth where blue is out and yellow in. [1]

Abstract

The main focus of this project is the continued study of a reversal of the earth's magnetic field recorded from lavas in the Liverpool Range of New South Wales, Australia. This reverse-to-normal transition, recently dated at ~40 Ma, was first reported in *Nature* in 1986. [2] In March 2011 some 200+ cores were drilled from several sections about the volcanic range—Jemmy's Creek, Bald Hill, Rock Creek, Yarraman, and Coolah Tops Road. Here we focus on paleomagnetic findings from samples drilled from the most extensive section, that being along the trail near Jemmy's Creek. Results from alternating field demagnetization show the earth's magnetic field was in the reverse direction for all 24 distinct lava outcrops sampled as well as some interesting behavior. The project also involved the rewriting and development of our software in FORTRAN 77 code in order for our output data to be compatible with an existing modern freeware program capable of graphing paleomagnetic analyses and plotting the results.

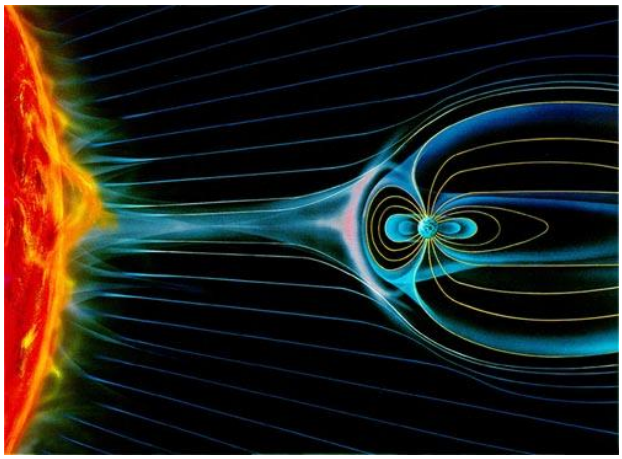

Figure 2: Depiction of Earth's magnetic field lines. [3]

Introduction

The Earth's magnetic field displays two polarities, normal, like the field of today when a free compass needle points north, and reverse, at those times when a free compass needle would have pointed south. The actual mechanism by which such transitions occur is poorly understood, although it is well understood that the field is generated in the highly electrical conducting fluid of the outer core. Nonetheless we can explore the process through paleomagnetic study.

Volcanic rocks such as the basaltic lavas erupted along the Liverpool Range record the direction of Earth's magnetic field while cooling to room temperature. When the temperature of the lava is above the Curie temperature (T_C) , thermal energy dominates and any magnetic grains within cannot hold any particular direction. As the lava cools however, more and more magnetic grain directions start to line up with the dominant external magnetic field. Usually, the dominant field is the Earth's dipole field.

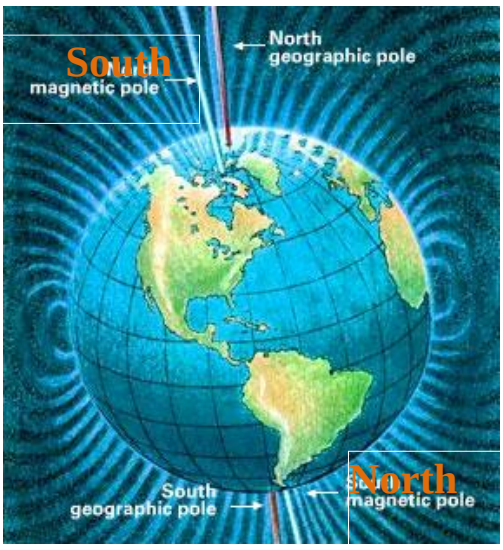

Figure 3: Normal dipole field direction [4].

Currently the earth's field is in the normal direction which means the magnetic north pole is down by the geographic South Pole as defined in physics. As my research will show, this is not always the case. The poles can either die out and come back as reversed or the magnetic South pole wanders south past the equator down to magnetic North and visa versa. It is hard to say which scenario actually happens because modern science has never had the chance to observe a reversal. A virtual geomagnetic pole (VGP) can be calculated using the direction of magnetization found in a rock sample and shows if the earth's field was reversed, normal, or in a transition.

Basics of Rock Magnetism

For rocks to hold a magnetic direction they must contain ferromagnetic minerals. Ferromagnetism is named after Fe (Fe is ferrum in Latin) because it's the most magnetic atom due to its atomic structure. However, there is a distinction between ferromagnetic and ferrimagnetic. Ferromagnetic refers to materials that contain magnetic directions that are all contributing to the total direction. Ferrimagnetic refers to magnetic directions that are not uniform. Some ions within have spins that flip up while others flip down, resulting in a net magnetic direction for the material that is either up or down. Below is a great example of ferrimagnetism from Butler. [5]

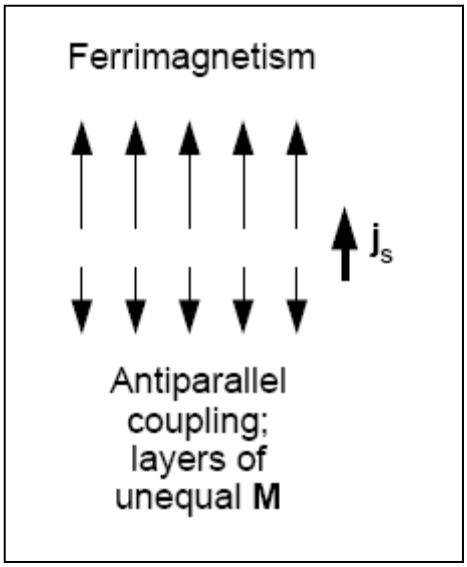

Figure 4: Ferrimagnetism giving a net upward direction.

Rocks containing titanomagnetites, a mix between magnetite (Fe_3O_4) and ulvöspinel (Fe_2TiO_4), like the basaltic rock from lava flows are rich in ferrimagnetic minerals. When ferrimagnetic minerals are raised above the T_C they become paramagnetic (The magnetization vector **m** is linearly dependant on an applied external magnetic field **H** and drops to zero without an applied **H** present).

The ferrimagnetic minerals within the basalts form grains from smaller than $1x10^{-6}$ meters (1 micron) to larger than 100 microns. However, grain sizes larger than 100 microns usually breakdown into multidomain grains. If this happens the much larger **m** contained in grains > 100 microns gets split up into many smaller magnetizations resulting in an overall weaker **m**. Hence the largest grains ~ 100 microns give the strongest directions for remnant magnetization. The ability for the magnetic directions to align antipodal to a stronger external **H** depends on both the temperature and the magnitude of **H**. As the temperature drops below T_C remnant magnetization begins and the Earth's magnetic field direction is literally frozen into the rock. If the Earth's dipole field was in reverse polarity, that direction would be frozen in initially and will always be

the strongest direction, reverse or not. Then latter, as the Earth's dipole field flips back to normal some weaker grains may flip toward that direction. The end result, millions of years later, is rock with one strong **m** direction and usually quit a few random weaker **m** directions.

There are two ways to erase the weaker **m** directions caused by sitting in a changing environment for millions of years. To measure the natural remnant magnetization (NRM), the rock can be either thermally demagnetized or demagnetized using an alternating field (AF). To thermally demagnetize a rock you must heat it up in steps, measuring the magnetic direction after each step. Once the added on **m** is removed the NRM will be the only direction left and increasing to higher steps will stop effecting what direction the **m** is pointing. The AF method is cooler and is how my research was done. AF demagnetization also wipes out added on **m** in steps.

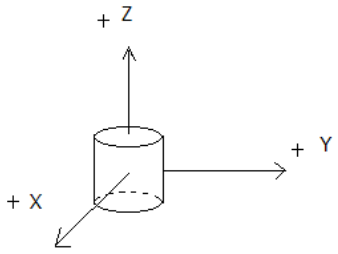

Figure 5; A sample cut from a lava flow core in Cartesian coordinates (~2cm x 2 cm).

The idea is to take a sample, initially apply a weak field that goes back and forth in the *X*-direction, then *Y*, then *Z*. This forces grains holding the weakest **m** directions to randomly flip to the + *X* or – *X* direction resulting in a 50% probability they flip to + *X* and 50% probability they flip to – *X* so that they cancel each other out leaving the stronger **m** in the *X*-direction, and the same happens for *Y* and *Z* directions. After the NRM is all that is left,

the direction stops changing and the NRM itself gets weaker in magnitude with increasing steps which can easily be seen in an orthogonal plot (See **Data and Analysis**).

Reversals and the Liverpool range of NSW, Australia

Figure 5; The Liverpool Range in NSW, Australia [6].

The Liverpool range is full of ancient volcanoes and kangaroos, but the reason for collecting samples here was because Prof. Hoffman of Cal Poly State University San Luis Obispo, my senior project advisor, had previously collected some samples from these mountains which showed reversal activity and he needed to do a more extensive sampling of the area to get the full picture of the reversal activity in the area from ~40 Ma. This senior project is focused on Jemmy's Creek but we took samples from many other locations.

Figure 6; Jemmy's Creek: Prof. Hoffman, Pierre Camps, Joe Dierkhising (from front to back).

Camps is a collaborator from France who studies the paleo-intensities from lava cores. Dierkhising is an earth science major and my lab partner for this senior project.

Figure 7; Rocky Creek.

Figure 8; Kangaroos.

Figure 9; Bald Hill.

Figure 10; Coolah Tops road.

Figure 11; Yarraman.

Collecting Samples

The main equipment needed for collecting samples were:

- Water cooled hole saw (ECHO 280E)
- Brunton Compass w/ Pomeroy orientation device
- Field notebook
- GPS
- Hammer and pin (for breaking samples free)

Samples were collected from Jemmy's Creek starting from the top too the bottom, a 2 hour hike down the mountain. As we walked down the mountain trail we took core samples from each outcrop of a distinct lava flow.

Step 1 – Drilling out a core. Notice in figure 11 below an initial circular mark is drilled into the rock for orientation.

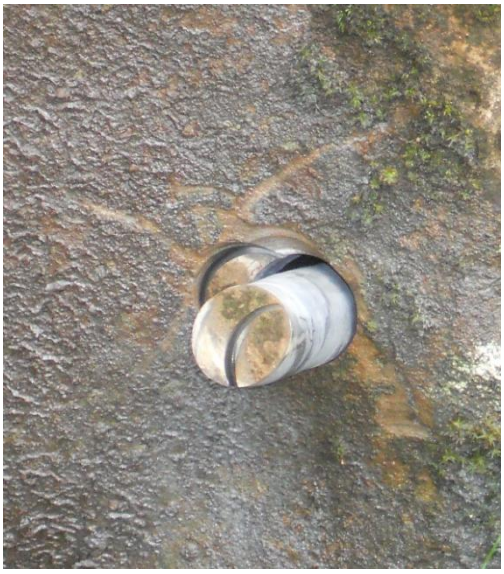

Figure 12; Sample marked before drilling it out.

Step 2 – We measure the natural orientation of the core with respect to the sun and magnetic north using the Brunton compass, noting the angle from north α, the tilt or dip β, date, time, and sundial reading. Then a brass wire (because it's non-magnetic) is

rubbed along a gap on the side of the Pomeroy to mark the core with respect to the compass. Then the core is popped out by tapping a pin into the side of the core. If we're lucky the core will crack off in one piece, otherwise cores are glued together back at the lab. Finally, the core is marked with a permanent marker that will tell us what site, what flow, and what core it is. For Jemmy's Creek the marking would look like "JC21-3," to show it is from Jemmy's Creek and that it is the third core from the twenty-first flow. For individual 2cm samples an *A* is tagged onto the end (JC21-3A) to indicate it is the deepest part of the core, then a *B* for the next 2cm, then *C* and so on. The last piece cut closest to the top, however, gets a *T*. The *T*'s are the most susceptible to weathering and are thus analyzed the least.

Figure 13; Brunton compass inside Pomeroy orientation device.

Step 3- We record *absolutely* everything in our field notebook, including what the site looks like to better explain later laboratory results if needed.

At least 3 cores must be taken from the same lava flow to estimate a direction for that flow by calculating a Fisher mean that needs at least two sample directions. Another reason for taking numerous samples is because some cores may have been damaged by unforeseen conditions like weathering, chemical processes, or lightning strikes that could throw off the actual remnant magnetization for a single core. A great example of this is the JC5 flow where 4 cores were analyzed [figure 26].

Lab Experiment and Procedure

The cores are cut into 2 cm pieces that fit inside a plastic cube designed for use with the spinner magnetometer.

Figure 14; cut sample with holding cube ready for analysis.

Figure 15; The spinner magnetometer averages the *m* for each side of the cube.

Samples are at first measured without demagnetization, this is the first step and after each side is measured the data is stored in a text file as M000. The *M* tells the experimenter that the sample is being AF demagnetized. If it was thermally demagnetized it would be a *T*. After the first step, the sample is demagnetized using an AF of magnitude 10 x 10^{-3} Teslas (10 mT).

Figure 16; Demagnetizer.

The Demagnetizer is a coil that uses an AC current to create an alternating magnetic flux inside a shield that blocks the Earth's magnetic field. The sample is then put back in the

spinner and the data is saved in a text file as M010 to show it has been demagnetized to 10 mT. If the sample behaves normal this procedure continues in steps of 10 mT until a final direction can be determined or until the 50 mT step is reached. After 50 mT is reached demagnetizing the rock will not be effective anymore as 50 mT is very strong for rocks. If the data looks questionable steps shrink to 5 mT increments to get a better picture of how well the sample is being demagnetized.

I began this project with a Fortran 77 program that took the data from the text files and derived the direction of **m** in Cartesian coordinates but only plotted in a dos command window. After learning how to program in FORTRAN, we found a freeware program online from the geological survey of Canada called PMGSC by Randy Enkin. The FORTRAN program was then altered so that it output all the data necessary for PMGSC in a file with compatible format. This allowed for easy viewing of all future results.

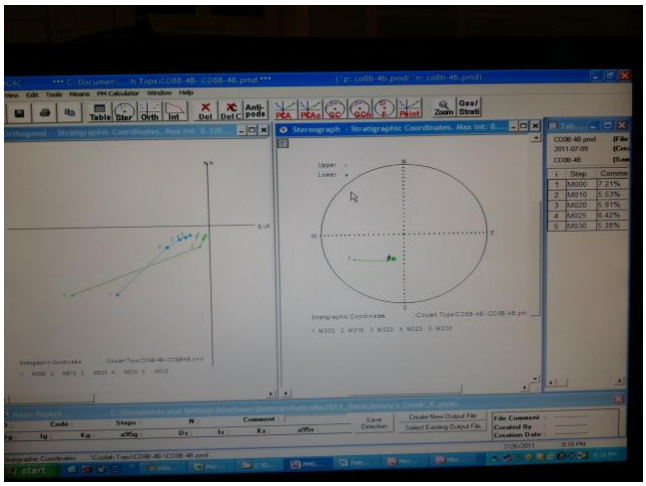

Figure 17; Display of the PMGSC program after demagnetizing a sample.

The window on the left in figure 17 is called an orthogonal view of the samples **m** direction on axis' North/South and East/West (and up/down respectively). Once the

sample only contains the NRM, new data points go straight to the origin. The window in the middle is a stereographic plot of the **m** direction and needs explaining. Imagine the sample is placed inside a glass sphere. Each data point on the sphere is the direction **m** is pointing. To account for not knowing if you are looking at a data point on the top or bottom of the sphere, bottom data points are displayed as green and top ones blue. The center window is showing a sample with a **m** that was at first pointing to the left and down but after one demagnetization step moved and stayed in a final direction much farther away. For Jemmy's Creek, three samples from each flow (but different cores) were analyzed one at a time using the PMGSC program.

For each flow there are at least three data points that should show a similar direction. The PMGSC program can then calculate a Fisher mean direction with error circles called the α95 which indicates there is a 95% confidence the true direction lies within the circle. The α95 can also be thought of as two standard deviations from the mean direction. An α95 of 10 is considered a bit high but acceptable in paleomagnetics.

The Butler book not only covers the basics of paleomagnetism, such as how the remnant magnetization sets up within the rock, but also goes on to give the equations needed to find the VGP position in latitude and longitude from a samples magnetic declination and inclination. The declination is how far away the **m** is from north from 0 to 360 degrees. The Inclination is how many degrees tilt the **m** is from earth's surface. Positive inclinations point downward. Here are the equations from Butler [5] chapter 7, which were used in our Matlab code to plot the VGPs.

$$p = \cot^{-1}\left(\frac{\tan I_m}{2}\right) = \tan^{-1}\left(\frac{2}{\tan I_m}\right) \quad (7.1)$$

Figure 18: *p* is the colatitude from site to VGP, where I_m is the samples inclination.

$$\lambda_p = \sin^{-1}\left(\sin\lambda_s \cos p + \cos\lambda_s \sin p \cos D_m\right) \quad (7.2)$$

Figure 19: subscript *p* denotes pole latitude, *s* is for site latitude, and D is the samples declination.

$$\beta = \sin^{-1}\left(\frac{\sin p \sin D_m}{\cos\lambda_p}\right)$$

Figure 20: Beta is the difference in longitude from site to VGP position.

$$\phi_p = \phi_s + \beta \quad (7.5)$$

Figure 21: Phi represents longitude. The *p* and *s* are for pole and site respectively.

Data and Analysis

JC1

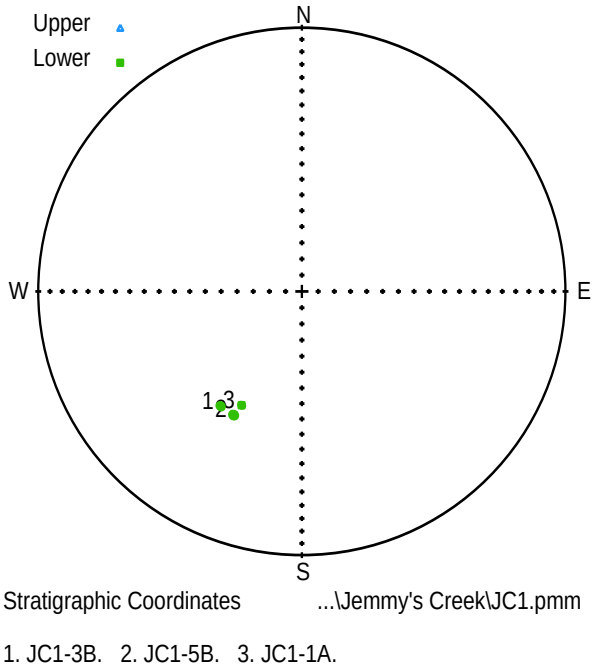

Figure 22: Site Inclinations and Declinations for JC 1.

*Note: the kg data is a parameter for Fisher means where higher means more reliable.

"JC1 averaged of 3 samples"
"JC1","Nathan Padilla","2011-07-26"
ID, CODE, STEPRANGE, N, Dg, Ig, kg, α95g, Ds, Is, ks, α95s,

JC1-3B., DirOPCA, M020-M030, 2, 215.3, 45.7, 0, 1.2, 215.3, 45.7, 0, 1.2, ""
JC1-5B., DirOPCA, M010-M040, 4, 208.9, 45.5, 0, 1.3, 208.9, 45.5, 0, 1.3, ""
JC1-1A., DirOPCA, M010-M040, 5, 207.9, 49.6, 0, 1.0, 207.9, 49.6, 0, 1.0, ""
JC1, Watson, site avg, 3, 210.8, 47.0, 382.3, 2.9, 210.8, 47.0, 382.3, 2.9, ""

JC2

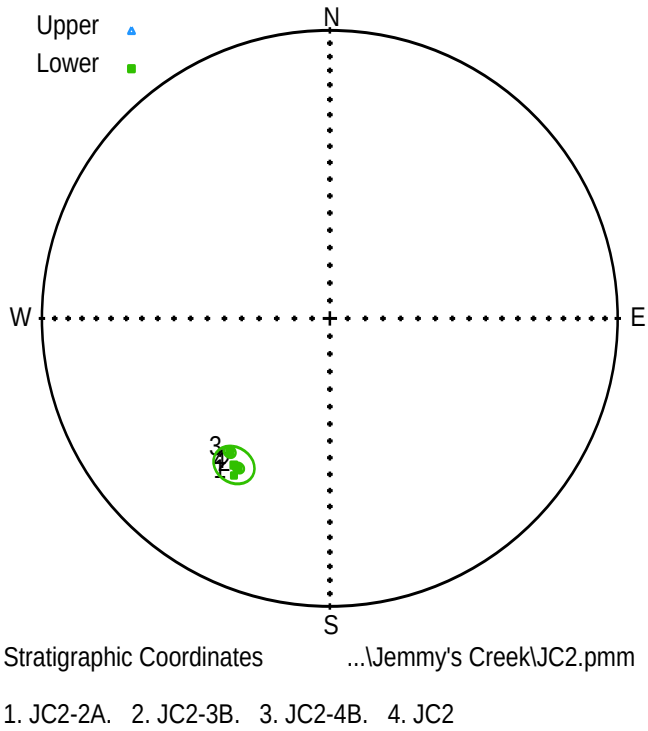

Figure 23: Site Inclinations and Declinations for JC 2 with Fisher mean and α95 circle.

"JC2","N.P.","2011-07-26"

ID, CODE, STEPRANGE, N, Dg, Ig, kg, α95g, Ds, Is, ks, α95s,

JC2-2A., DirOPCA, M020-M040, 4, 211.4, 36.3, 0, 0.5, 211.4, 36.3, 0, 0.5, ""

JC2-3B., DirOPCA, M010-M030, 3, 211.5, 39.0, 0, 1.5, 211.5, 39.0, 0, 1.5, ""

JC2-4B., DirOPCA, M010-M040, 4, 216.9, 41.6, 0, 1.6, 216.9, 41.6, 0, 1.6, ""

JC2, Fisher, site avg, 3, 213.2, 39.0, 509.5, 5.5, 213.2, 39.0, 509.5, 5.5, ""

JC3

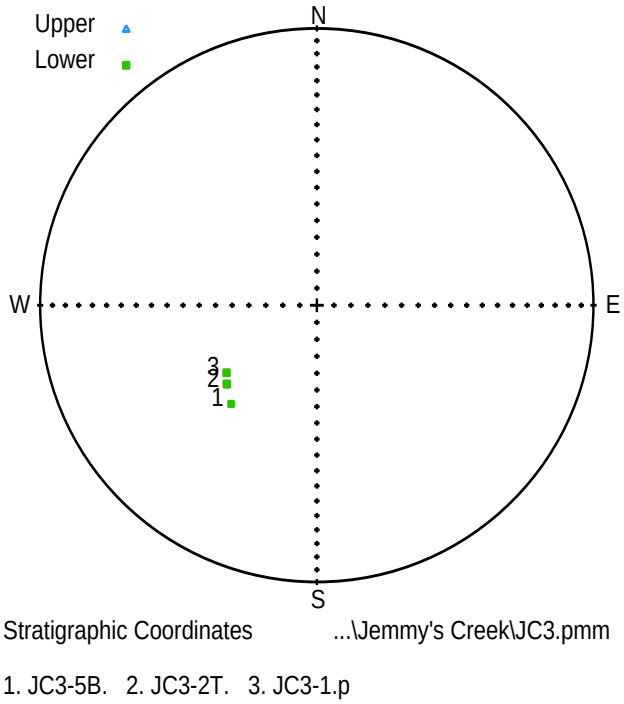

Figure 24: Site Inclinations and Declinations for JC 3.

"JC3","N.P.","2011-07-26"
ID, CODE, STEPRANGE, N, Dg, Ig, kg, α95g, Ds, Is, ks, α95s,

JC3-5B., DirOPCA, M010-M040, 4, 221.0, 51.0, 0, 0.6, 221.0, 51.0, 0, 0.6, ""
JC3-2T., DirOPCA, M010-M030, 3, 228.8, 54.4, 0, 0.9, 228.8, 54.4, 0, 0.9, ""
JC3-1.p, DirOPCA, M030-M040, 2, 233.2, 56.5, 0, 0.6, 233.2, 56.5, 0, 0.6, ""
JC3, Fisher, site avg, 3, 227.4, 54.1, 311.9, 7.0, 227.4, 54.1, 311.9, 7.0, ""

JC4

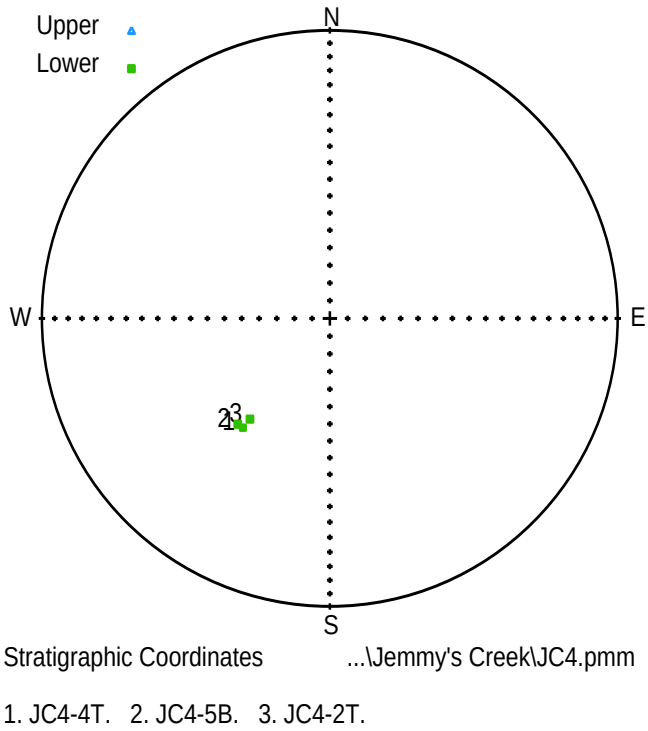

Figure 25: Site Inclinations and Declinations for JC 4.

"JC4","N.P.","2011-07-26"
ID, CODE, STEPRANGE, N, Dg, Ig, kg, α95g, Ds, Is, ks, α95s,

JC4-4T., DirOPCA, M010-M030, 4, 218.5, 49.9, 0, 0.6, 218.5, 49.9, 0, 0.6, ""
JC4-5B., DirOPCA, M010-M030, 3, 221.0, 49.7, 0, 0.3, 221.0, 49.7, 0, 0.3, ""
JC4-2T., DirOPCA, M010-M030, 3, 218.4, 53.2, 0, 0.2, 218.4, 53.2, 0, 0.2, ""
JC4, Fisher, site avg, 3, 219.3, 50.9, 1386.8,3.3, 219.3, 50.9, 1386.8,3.3, ""

JC5

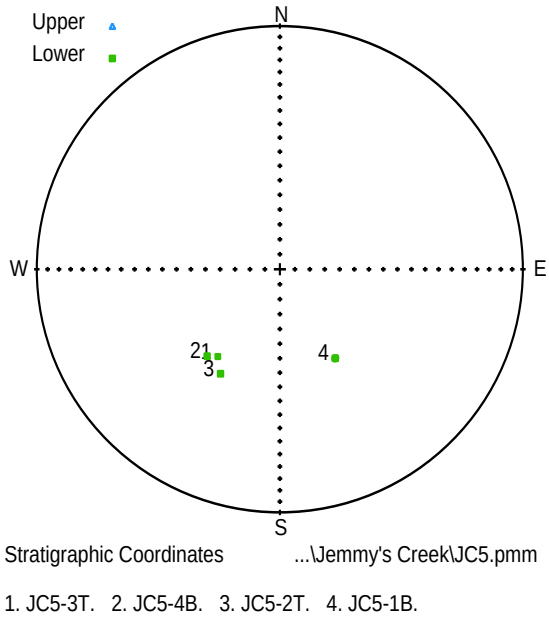

Figure 26: Site Inclinations and Declinations for JC 5. Core JC5-1B is an outlier (anomaly/bad data).

"JC5","N.P.","2011-07-26"

ID, CODE, STEPRANGE, N, Dg, Ig, kg, α95g, Ds, Is, ks, α95s,

JC5-3T., DirOPCA, M010-M040, 4, 215.4, 53.7, 0, 0.4, 215.4, 53.7, 0, 0.4, ""

JC5-4B., DirOPCA, M010-M040, 4, 219.9, 51.5, 0, 0.3, 219.9, 51.5, 0, 0.3, ""

JC5-2T., DirOPCA, M030-M040, 2, 209.6, 49.1, 0, 0.2, 209.6, 49.1, 0, 0.2, ""

JC5-1B., DirOPCA, M045-M050, 2, 148.1, 54.5, 0, 1.0, 148.1, 54.5, 0, 1.0, ""

JC5, Fisher, site avg, 3, 214.9, 51.5, 412.8, 6.1, 214.9, 51.5, 412.8, 6.1, ""

JC6

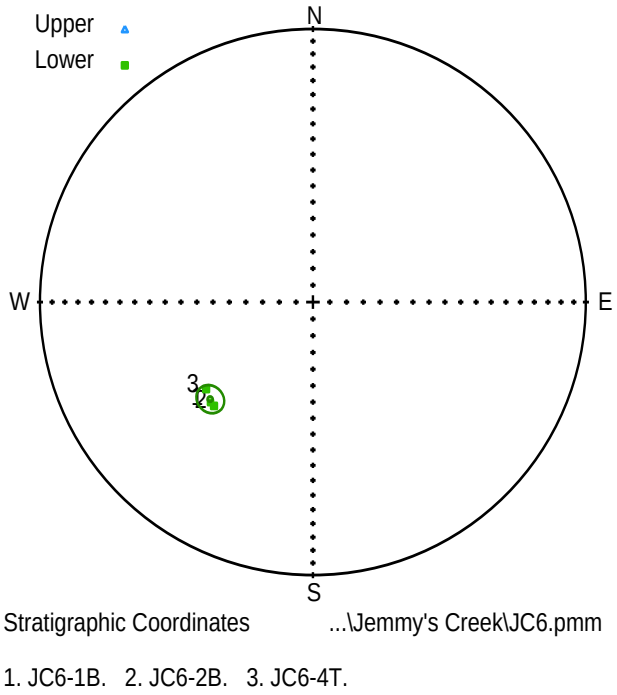

Figure 27: Site Inclinations and Declinations for JC 6 with Fisher mean and α95 circle.

"JC6","N.P.","2011-07-26"

ID, CODE, STEPRANGE, N, Dg, Ig, kg, α95g, Ds, Is, ks, α95s,

JC6-1B., DirOPCA, M000-M040, 4, 225.6, 46.4, 0, 0.2, 225.6, 46.4, 0, 0.2, ""

JC6-2B., DirOPCA, M000-M030, 4, 223.6, 46.4, 0, 0.3, 223.6, 46.4, 0, 0.3, ""

JC6-4T., DirOPCA, M010-M030, 3, 230.8, 48.2, 0, 0.2, 230.8, 48.2, 0, 0.2, ""

JC6, Fisher, site avg, 3, 226.6, 47.0, 883.0, 4.2, 226.6, 47.0, 883.0, 4.2, ""

JC7

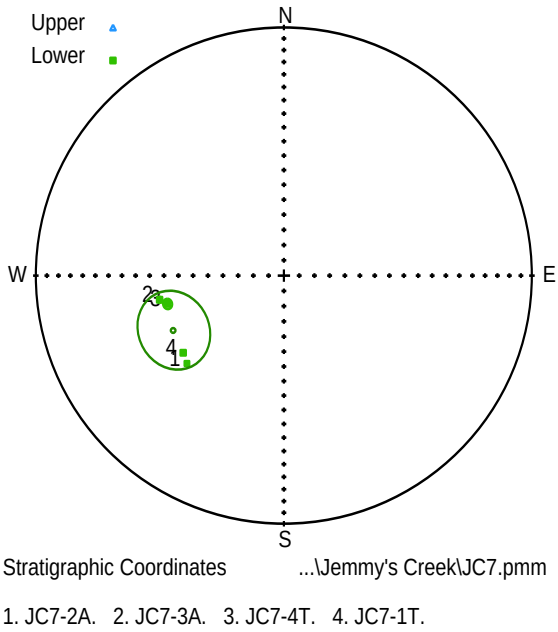

Figure 28: Site Inclinations and Declinations for JC 7 with Fisher mean and α95 circle.

"JC7","N.P.","2011-07-26"
ID, CODE, STEPRANGE, N, Dg, Ig, kg, α95g, Ds, Is, ks, α95s,

JC7-2A., DirOPCA, M020-M030, 2, 227.8, 46.2, 0, 0.3, 227.8, 46.2, 0, 0.3, ""
JC7-3A., DirOPCA, M030-M050, 3, 259.0, 47.7, 0, 0.9, 259.0, 47.7, 0, 0.9, ""
JC7-4T., DirOPCA, M030-M045, 3, 256.3, 50.1, 0, 1.6, 256.3, 50.1, 0, 1.6, ""
JC7-2T., DirOPCA, M020-M040, 3, 226.3, 45.0, 0, 0.5, 226.3, 45.0, 0, 0.5, ""
JC7-1T., DirOPCA, M010-M030, 3, 232.5, 47.6, 0, 0.4, 232.5, 47.6, 0, 0.4, ""
JC7-3B., DirOPCA, M030-M040, 2, 254.5, 44.8, 0, 0.5, 254.5, 44.8, 0, 0.5, ""
JC7, Fisher, site avg, 4, 243.6, 48.7, 56.1, 12.4, 243.6, 48.7, 56.1, 12.4, "

JC8

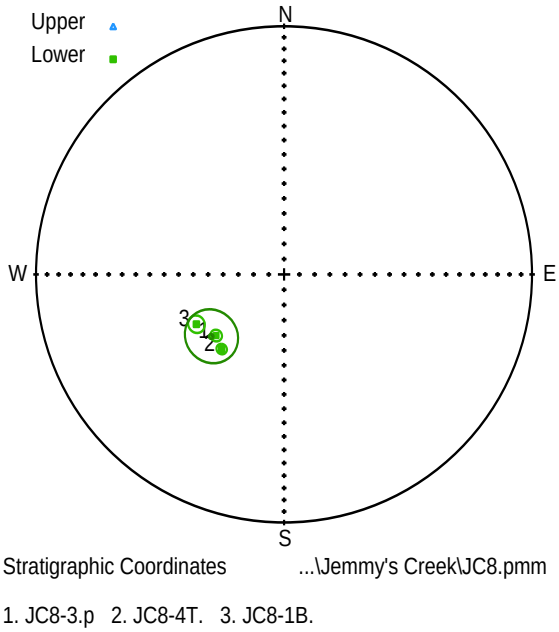

Figure 29: Site Inclinations and Declinations for JC 8 with Fisher mean and α95 circle.

"JC8","N.P.","2011-08-14"
ID, CODE, STEPRANGE, N, Dg, Ig, kg, α95g, Ds, Is, ks, α95s,

JC8-3.p, DirOPCA, M030-M050, 3, 228.0, 59.8, 0, 1.9, 228.0, 59.8, 0, 1.9, ""
JC8-4T., DirOPCA, M045-M050, 2, 219.9, 57.8, 0, 1.7, 219.9, 57.8, 0, 1.7, ""
JC8-1B., DirOPCA, M030-M040, 2, 239.2, 56.7, 0, 2.0, 239.2, 56.7, 0, 2.0, ""
JC8-1B., DirOPCA, M030-M050, 3, 240.4, 56.6, 0, 2.8, 240.4, 56.6, 0, 2.8, ""
JC8, Fisher, site avg, 3, 229.6, 58.4, 199.0, 8.8, 229.6, 58.4, 199.0, 8.8, ""

JC9

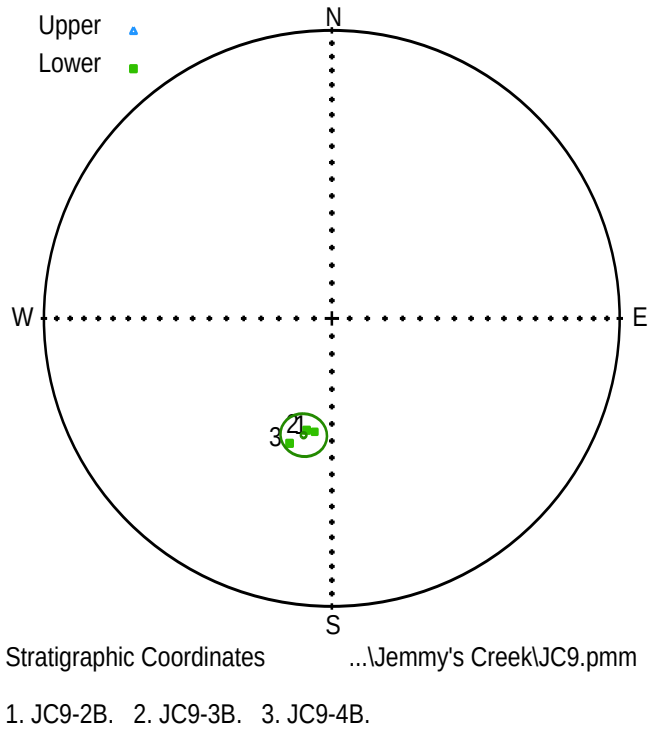

Figure 30: Site Inclinations and Declinations for JC 9 with Fisher mean and α95 circle.

"JC9","N.P.","2011-08-15"

ID,	CODE,	STEPRANGE,	N,	Dg,	Ig,	kg,	α95g,	Ds,	Is,	ks,	α95s,	
JC9-2B.,	DirOPCA,	M010-M030,	3,	188.6,	57.3,	0,	0.2,	188.6,	57.3,	0,	0.2,	""
JC9-3B.,	DirOPCA,	M010-M030,	3,	192.7,	57.3,	0,	0.3,	192.7,	57.3,	0,	0.3,	""
JC9-4B.,	DirOPCA,	M010-M030,	3,	198.7,	52.2,	0,	0.3,	198.7,	52.2,	0,	0.3,	""
JC9,	Fisher,	site avg,	3,	193.6,	55.7,	384.0,	6.3,	193.6,	55.7,	384.0,	6.3,	""

JC10

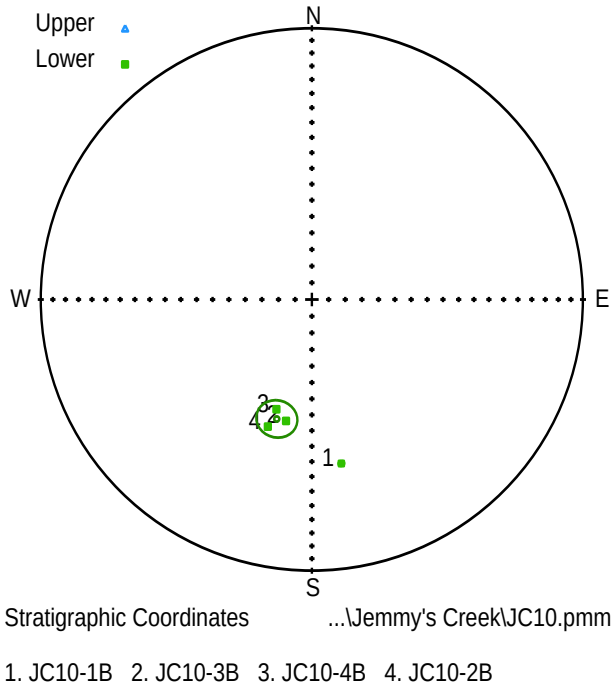

Figure 31: Site Inclinations and Declinations for JC 10 with Fisher mean and α95 circle.

"JC10","N.P.","2011-08-18"
ID, CODE, STEPRANGE, N, Dg, Ig, kg, α95g, Ds, Is, ks, α95s,

JC10-1B, DirOPCA, M010-M040, 4, 169.8, 38.5, 0, 0.8, 169.8, 38.5, 0, 0.8, ""
JC10-3B, DirOPCA, M010-M030, 3, 192.0, 52.2, 0, 0.4, 192.0, 52.2, 0, 0.4, ""
JC10-4B, DirOPCA, M010-M040, 4, 197.9, 55.0, 0, 0.4, 197.9, 55.0, 0, 0.4, ""
JC10-2B, DirOPCA, M010-M030, 3, 199.1, 48.9, 0, 0.3, 199.1, 48.9, 0, 0.3, ""
JC10, Fisher, site avg, 3, 196.4, 52.1, 442.5, 5.9, 196.4, 52.1, 442.5, 5.9, ""

JC11

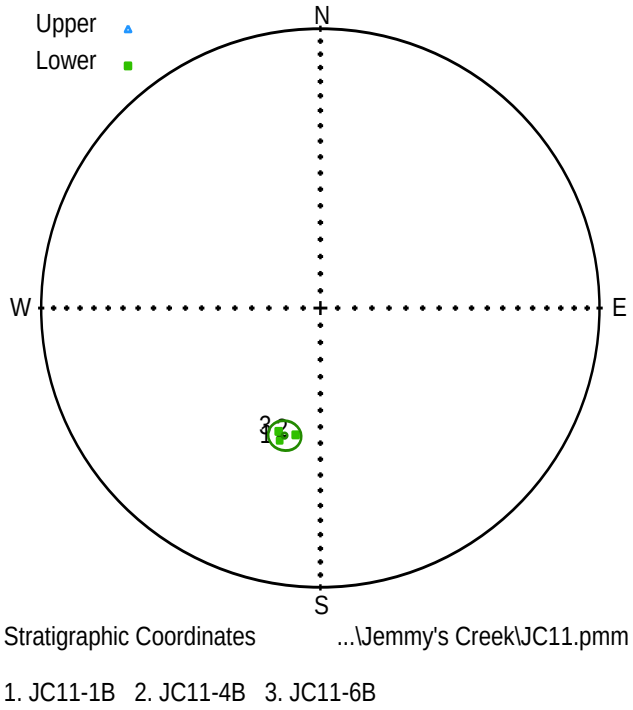

Figure 32: Site Inclinations and Declinations for JC 11 with Fisher mean and α95 circle.

"JC11","N.P.","2011-08-18"
ID, CODE, STEPRANGE, N, Dg, Ig, kg, α95g, Ds, Is, ks, α95s,

JC11-1B, DirOPCA, M010-M030, 3, 197.1, 48.9, 0, 0.4, 197.1, 48.9, 0, 0.4, ""
JC11-4B, DirOPCA, M010-M030, 3, 191.0, 51.8, 0, 0.5, 191.0, 51.8, 0, 0.5, ""
JC11-6B, DirOPCA, M010-M030, 3, 198.7, 51.5, 0, 0.2, 198.7, 51.5, 0, 0.2, ""
JC11, Fisher, site avg, 3, 195.6, 50.8, 726.4, 4.6, 195.6, 50.8, 726.4, 4.6, ""

JC12

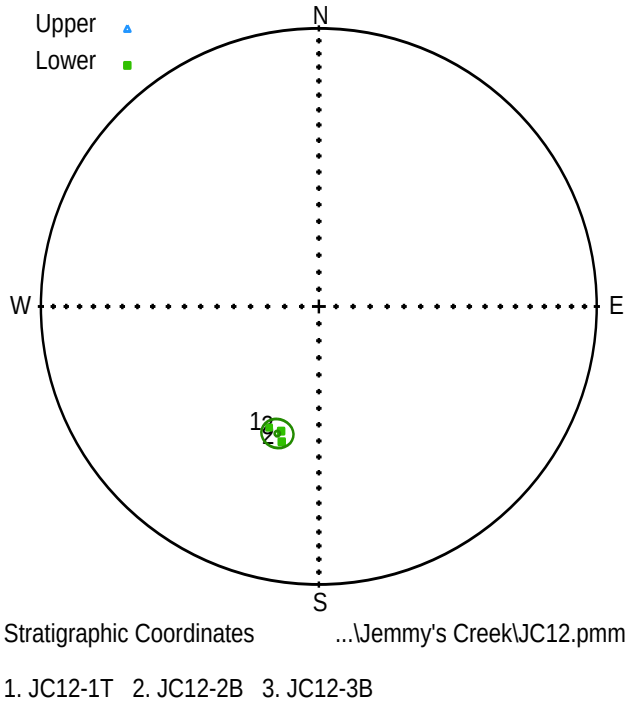

Figure 33: Site Inclinations and Declinations for JC 12 with Fisher mean and α95 circle.

"JC12","N.P.","2011-08-18"
ID, CODE, STEPRANGE, N, Dg, Ig, kg, α95g, Ds, Is, ks, α95s,

JC12-1T, DirOPCA, M010-M030, 3, 202.3, 51.1, 0, 0.3, 202.3, 51.1, 0, 0.3, ""
JC12-2B, DirOPCA, M010-M030, 3, 195.3, 48.2, 0, 0.2, 195.3, 48.2, 0, 0.2, ""
JC12-3B, DirOPCA, M010-M030, 3, 196.8, 51.3, 0, 0.2, 196.8, 51.3, 0, 0.2, ""
JC12, Fisher, site avg, 3, 198.1, 50.2, 766.9, 4.5, 198.1, 50.2, 766.9, 4.5, ""

JC13

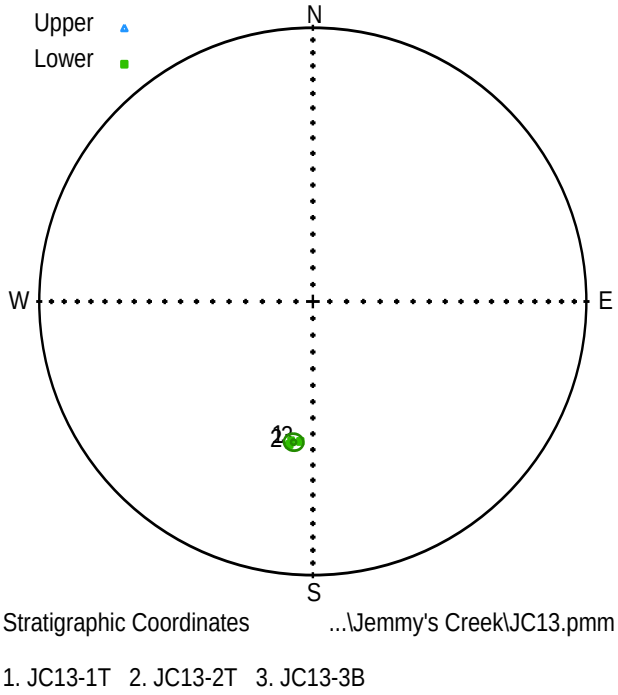

Figure 34: Site Inclinations and Declinations for JC 13 with Fisher mean and α95 circle.

"JC13","N.P.","2011-08-18"
ID, CODE, STEPRANGE, N, Dg, Ig, kg, α95g, Ds, Is, ks, α95s,

JC13-1T, DirOPCA, M010-M030, 3, 188.9, 47.4, 0, 0.4, 188.9, 47.4, 0, 0.4, ""
JC13-2T, DirOPCA, M010-M030, 3, 189.3, 46.0, 0, 0.3, 189.3, 46.0, 0, 0.3, ""
JC13-3B, DirOPCA, M010-M030, 3, 185.1, 47.4, 0, 0.1, 185.1, 47.4, 0, 0.1, ""
JC13, Fisher, site avg, 3, 187.8, 46.9, 2084.1,2.7, 187.8, 46.9, 2084.1,2.7, ""

JC14

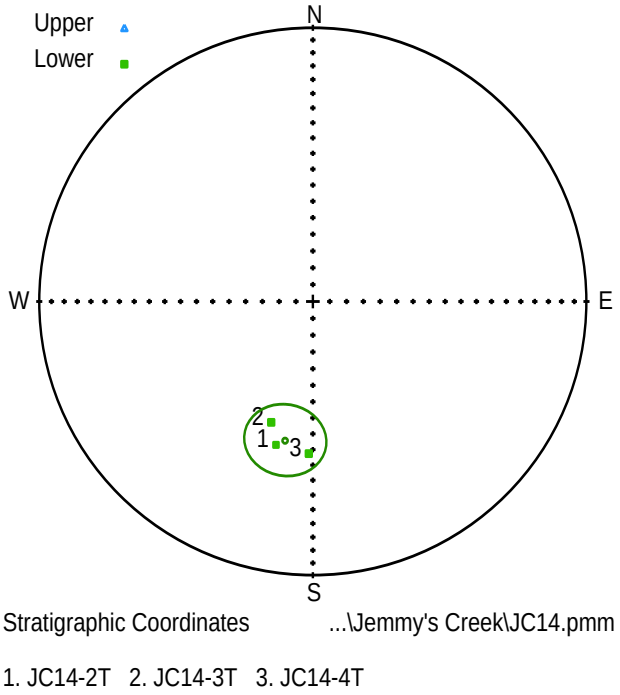

Figure 35: Site Inclinations and Declinations for JC 14 with Fisher mean and α95 circle.

"JC14","N.P.","2011-08-18"
ID, CODE, STEPRANGE, N, Dg, Ig, kg, α95g, Ds, Is, ks, α95s,

JC14-2T, DirOPCA, M010-M030, 3, 194.4, 45.0, 0, 0.4, 194.4, 45.0, 0, 0.4, ""
JC14-3T, DirOPCA, M010-M030, 3, 199.0, 51.4, 0, 0.5, 199.0, 51.4, 0, 0.5, ""
JC14-4T, DirOPCA, M020-M040, 3, 181.5, 43.7, 0, 0.4, 181.5, 43.7, 0, 0.4, ""
JC14, Fisher, site avg, 3, 191.3, 46.9, 118.0, 11.4, 191.3, 46.9, 118.0, 11.4, ""

JC15

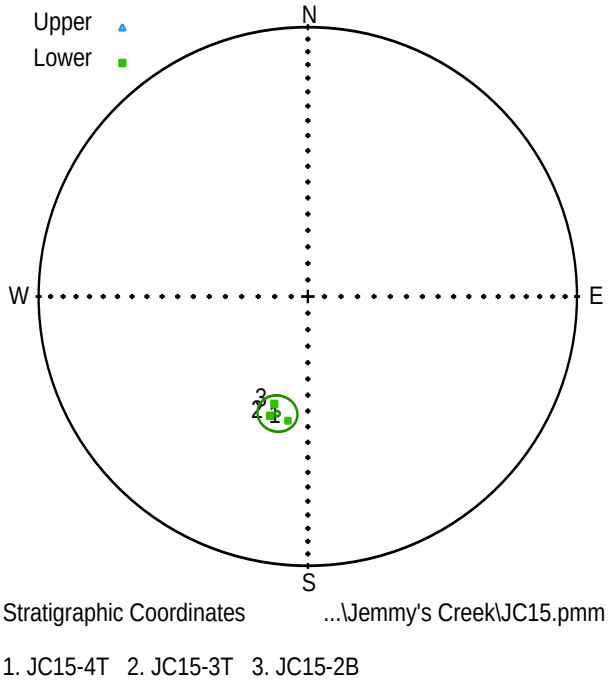

Figure 36: Site Inclinations and Declinations for JC 15 with Fisher mean and α95 circle.

"JC15","N.P.","2011-08-18"
ID, CODE, STEPRANGE, N, Dg, Ig, kg, α95g, Ds, Is, ks, α95s,

JC15-4T, DirOPCA, M010-M040, 4, 189.1, 51.4, 0, 0.3, 189.1, 51.4, 0, 0.3, ""
JC15-3T, DirOPCA, M010-M030, 3, 197.6, 51.6, 0, 0.3, 197.6, 51.6, 0, 0.3, ""
JC15-2B, DirOPCA, M010-M040, 3, 197.3, 55.6, 0, 0.4, 197.3, 55.6, 0, 0.4, ""
JC15, Fisher, site avg, 3, 194.6, 52.9, 461.4, 5.7, 194.6, 52.9, 461.4, 5.7, ""

JC16

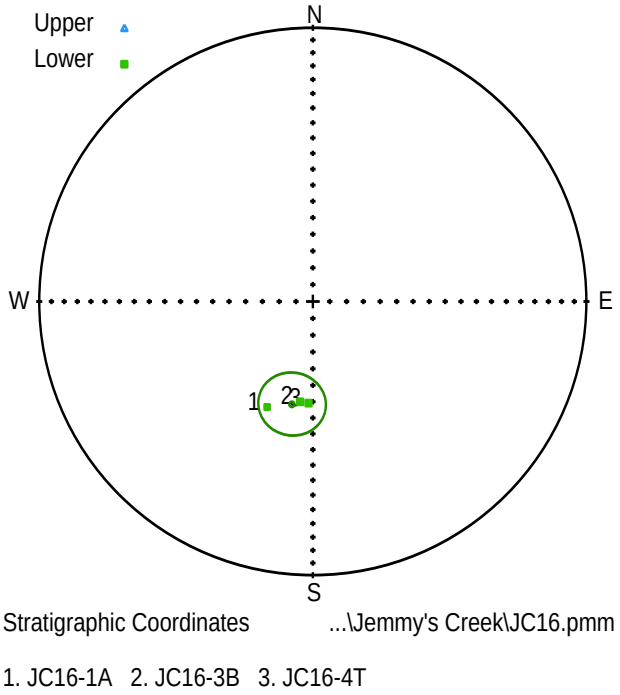

Figure 37: Site Inclinations and Declinations for JC 16 with Fisher mean and α95 circle.

"JC16","N.P.","2011-08-19"
ID, CODE, STEPRANGE, N, Dg, Ig, kg, α95g, Ds, Is, ks, α95s,

JC16-1A, DirOPCA, M000-M030, 4, 203.4, 55.4, 0, 0.1, 203.4, 55.4, 0, 0.1, ""
JC16-3B, DirOPCA, M010-M030, 3, 187.2, 59.7, 0, 0.6, 187.2, 59.7, 0, 0.6, ""
JC16-4T, DirOPCA, M010-M030, 3, 182.4, 59.5, 0, 0.1, 182.4, 59.5, 0, 0.1, ""
JC16, Fisher, site avg, 3, 191.5, 58.5, 162.7, 9.7, 191.5, 58.5, 162.7, 9.7, ""

JC17

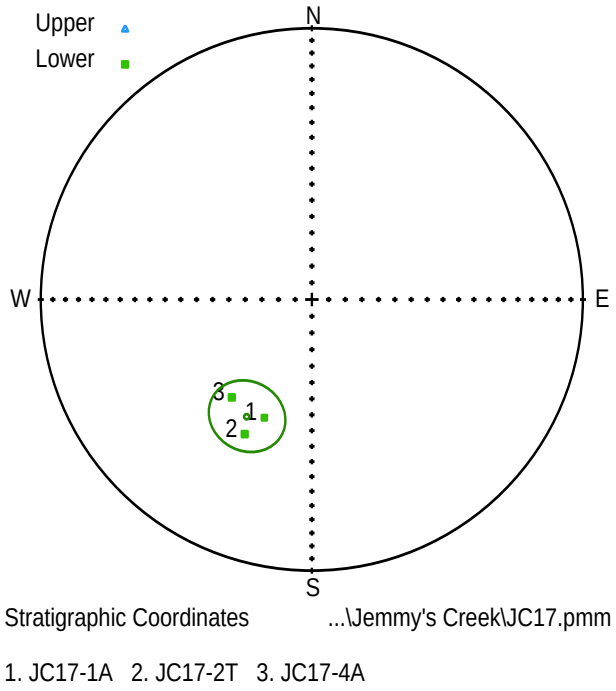

Figure 38: Site Inclinations and Declinations for JC 17 with Fisher mean and α95 circle.

"JC17","N.P.","2011-08-20"
ID, CODE, STEPRANGE, N, Dg, Ig, kg, α95g, Ds, Is, ks, α95s,

JC17-1A, DirOPCA, M010-M030, 3, 201.9, 51.2, 0, 0.3, 201.9, 51.2, 0, 0.3, ""
JC17-2T, DirOPCA, M000-M020, 3, 206.5, 43.8, 0, 0.2, 206.5, 43.8, 0, 0.2, ""
JC17-4A, DirOPCA, M010-M030, 3, 219.3, 51.5, 0, 0.5, 219.3, 51.5, 0, 0.5, ""
JC17, Fisher, site avg, 3, 209.1, 49.1, 125.1, 11.1, 209.1, 49.1, 125.1, 11.1, ""

JC18

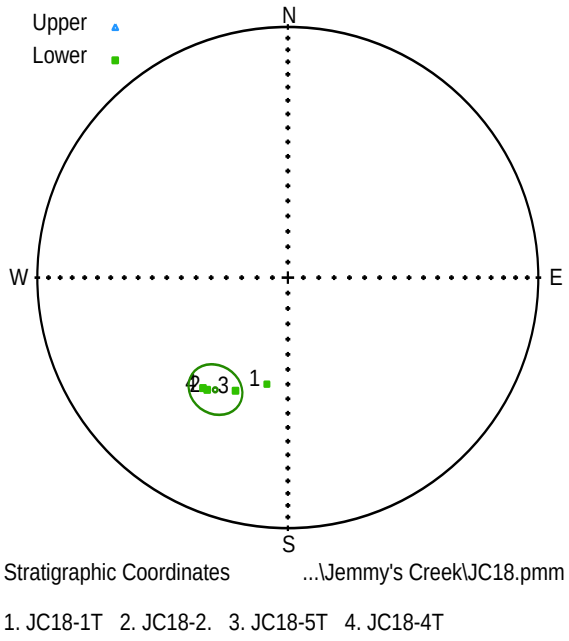

Figure 39: Site Inclinations and Declinations for JC 18 with Fisher mean and α95 circle.

"JC18","N.P.","2011-08-22"
ID, CODE, STEPRANGE, N, Dg, Ig, kg, α95g, Ds, Is, ks, α95s,

JC18-1T, DirOPCA, M020-M040, 3, 191.1, 54.3, 0, 0.2, 191.1, 54.3, 0, 0.2, ""
JC18-2., DirOPCA, M000-M030, 4, 215.7, 44.1, 0, 0.2, 215.7, 44.1, 0, 0.2, ""
JC18-5T, DirOPCA, M000-M030, 4, 204.8, 48.8, 0, 0.1, 204.8, 48.8, 0, 0.1, ""
JC18-4T, DirOPCA, M040-M050, 2, 217.5, 43.7, 0, 0.2, 217.5, 43.7, 0, 0.2, ""
JC18, Fisher, site avg, 3, 212.9, 45.7, 215.6, 8.4, 212.9, 45.7, 215.6, 8.4, ""

JC19

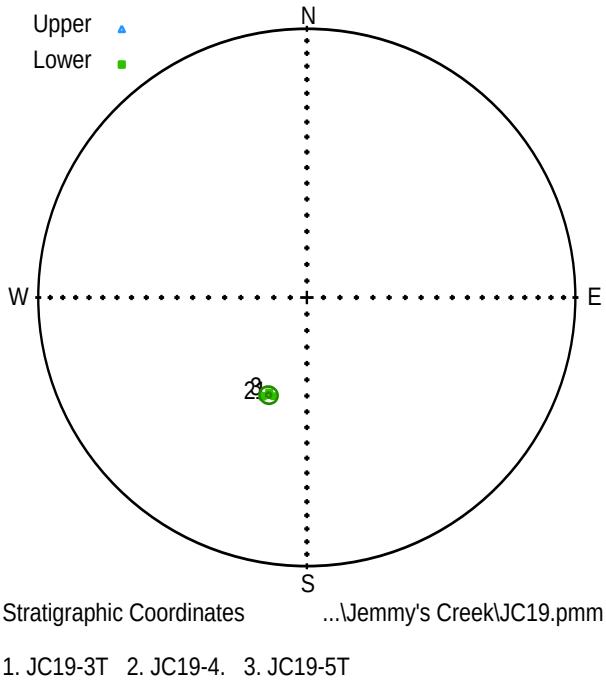

Figure 40: Site Inclinations and Declinations for JC 19 with Fisher mean and α95 circle.

"JC19","N.P.","2011-08-23"
ID, CODE, STEPRANGE, N, Dg, Ig, kg, α95g, Ds, Is, ks, α95s,

JC19-3T, DirOPCA, M000-M030, 3, 198.5, 58.2, 0, 0.4, 198.5, 58.2, 0, 0.4, ""
JC19-4., DirOPCA, M000-M030, 4, 204.1, 56.9, 0, 0.3, 204.1, 56.9, 0, 0.3, ""
JC19-5T, DirOPCA, M010-M030, 3, 201.5, 58.7, 0, 0.6, 201.5, 58.7, 0, 0.6, ""
JC19, Fisher, site avg, 3, 201.4, 58.0, 2119.9,2.7, 201.4, 58.0, 2119.9,2.7, ""

JC20

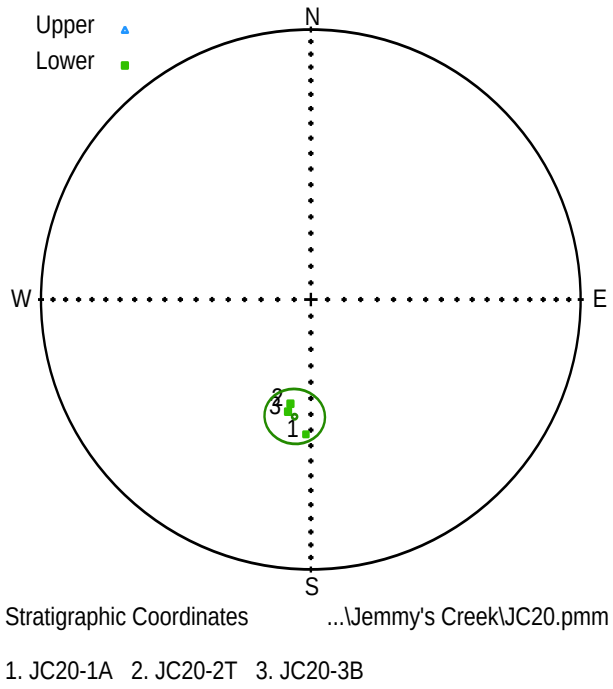

Figure 41: Site Inclinations and Declinations for JC 20 with Fisher mean and α95 circle.

"JC20","N.P.","2011-08-26"
ID, CODE, STEPRANGE, N, Dg, Ig, kg, α95g, Ds, Is, ks, α95s,

JC20-1A, DirOPCA, M000-M030, 4, 182.1, 48.6, 0, 0.2, 182.1, 48.6, 0, 0.2, ""
JC20-2T, DirOPCA, M010-M030, 3, 191.1, 57.7, 0, 0.1, 191.1, 57.7, 0, 0.1, ""
JC20-3B, DirOPCA, M010-M040, 4, 191.5, 55.1, 0, 0.2, 191.5, 55.1, 0, 0.2, ""
JC20, Fisher, site avg, 3, 187.9, 53.9, 203.2, 8.7, 187.9, 53.9, 203.2, 8.7, ""

JC21

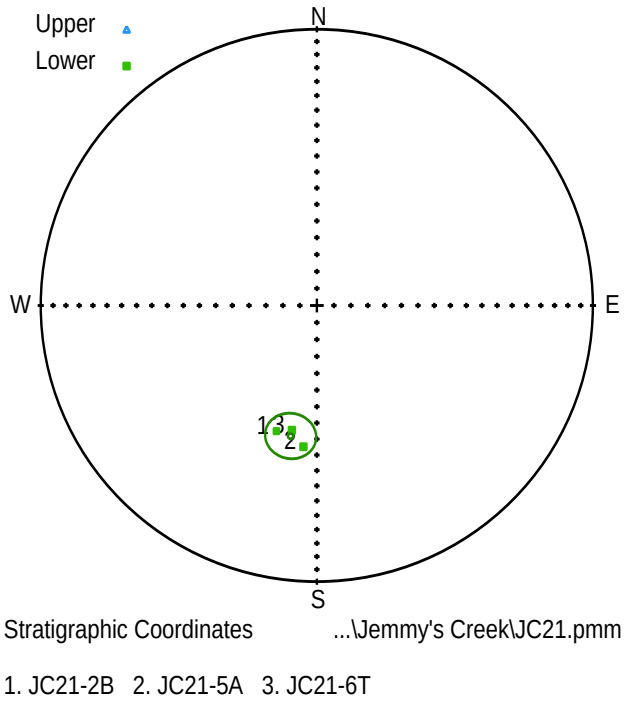

Figure 42: Site Inclinations and Declinations for JC 21 with Fisher mean and α95 circle.

"JC21","N.P.","2011-08-27"
ID, CODE, STEPRANGE, N, Dg, Ig, kg, α95g, Ds, Is, ks, α95s,

JC21-2B, DirOPCA, M000-M030, 4, 197.8, 50.5, 0, 0.1, 197.8, 50.5, 0, 0.1, ""
JC21-5A, DirOPCA, M000-M030, 4, 185.4, 47.4, 0, 0.2, 185.4, 47.4, 0, 0.2, ""
JC21-6T, DirOPCA, M000-M030, 4, 191.3, 52.0, 0, 0.2, 191.3, 52.0, 0, 0.2, ""
JC21, Fisher, site avg, 3, 191.4, 50.1, 302.8, 7.1, 191.4, 50.1, 302.8, 7.1, ""

JC22

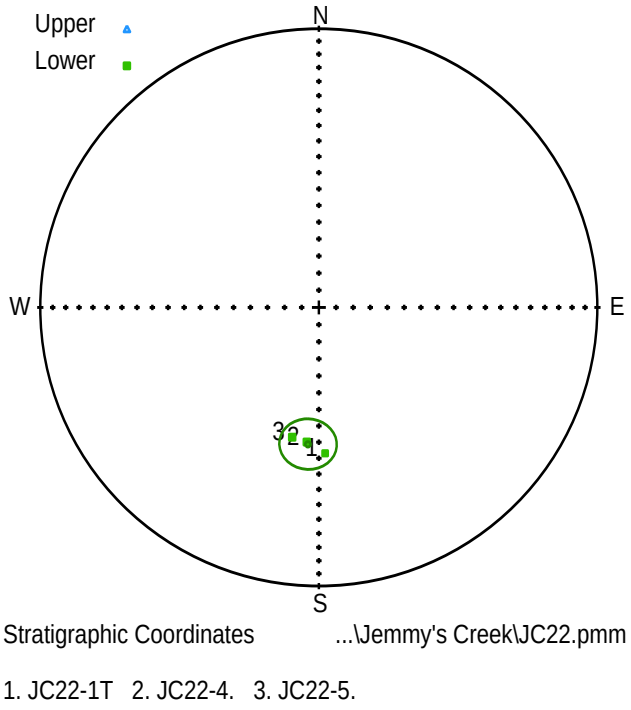

Figure 43: Site Inclinations and Declinations for JC 22 with Fisher mean and α95 circle.

"JC22","N.P.","2011-08-28"
ID, CODE, STEPRANGE, N, Dg, Ig, kg, α95g, Ds, Is, ks, α95s,

JC22-1T, DirOPCA, M000-M040, 5, 177.5, 46.5, 0, 0.4, 177.5, 46.5, 0, 0.4, ""
JC22-4., DirOPCA, M000-M030, 4, 185.1, 49.9, 0, 0.2, 185.1, 49.9, 0, 0.2, ""
JC22-5., DirOPCA, M000-M030, 4, 191.6, 50.7, 0, 0.2, 191.6, 50.7, 0, 0.2, ""
JC22, Fisher, site avg, 3, 184.5, 49.2, 247.6, 7.9, 184.5, 49.2, 247.6, 7.9, ""

JC23

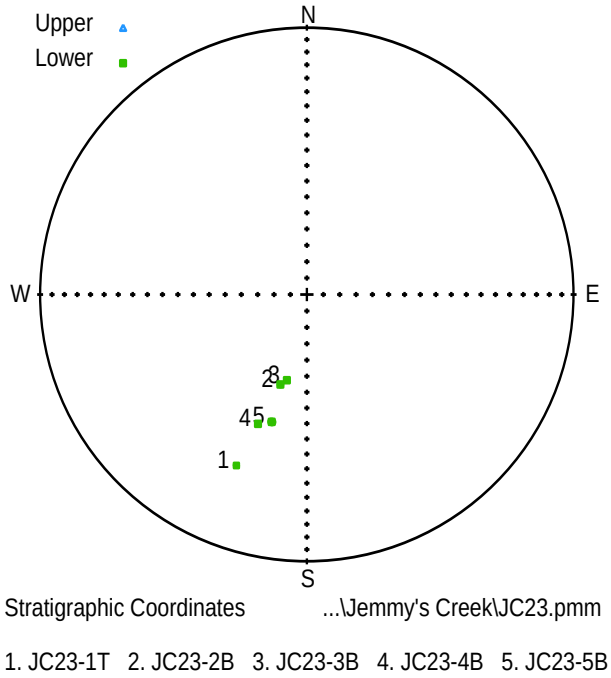

Figure 44: Site Inclinations and Declinations for JC 23. No 1 Fisher mean due to anomalous behavior.

"JC23","N.P.","2011-08-30"

ID,	CODE,	STEPRANGE,	N,	Dg,	Ig,	α95g
JC23-1T,	DirOPCA,	M010-M040,	4,	202.4,	31.3,	0.7
JC23-2B,	DirOPCA,	M000-M030,	4,	196.4,	61.2,	0.8
JC23-3B,	DirOPCA,	M000-M030,	4,	193.1,	63.0,	0.4
JC23-4B,	DirOPCA,	M020-M030,	2,	200.7,	47.0,	0.7
JC23-5B,	DirOPCA,	M010-M030,	3,	195.4,	49.0,	1.0
Fisher for JC23-2B & JC23-3B only.						
JC23,	Fisher,	site avg,	2,	194.8,	62.1,	5.2
Fisher for JC23-4B & JC23-5B only.						
JC23,	Fisher,	site avg,	2,	198.1,	48.0,	8.9

JC24A

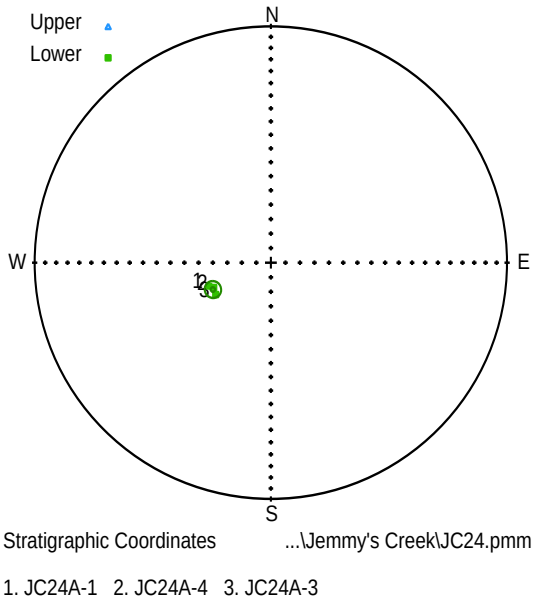

Figure 45: Site Inclinations and Declinations for JC 24A with Fisher mean and α95 circle.

"JC24A","N.P.","2011-08-31"
ID, CODE, STEPRANGE, N, Dg, Ig, kg, α95g, Ds, Is, ks, α95s, comment,
JC24A-1, DirOPCA, M010-M040, 4, 249.0, 67.2, 0, 0.5, 249.0, 67.2, 0, 0.5, ""
JC24A-4, DirOPCA, M010-M050, 5, 246.5, 68.5, 0, 0.5, 246.5, 68.5, 0, 0.5, ""
JC24A-3, DirOPCA, M020-M040, 3, 239.9, 68.0, 0, 0.2, 239.9, 68.0, 0, 0.2, ""
JC24A, Fisher, site avg, 3, 245.2, 67.9, 1837.6,2.9, 245.2, 67.9, 1837.6,2.9,

JC24B

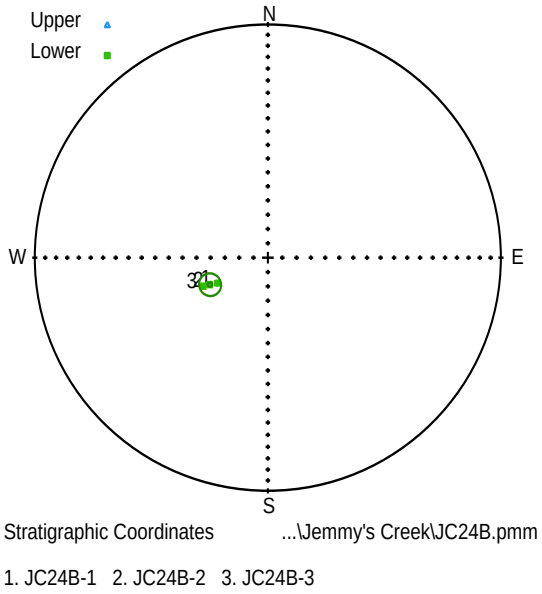

Figure 46: Site Inclinations and Declinations for JC 24B with Fisher mean and α95 circle.

"JC24B","N.P.","2011-09-01"
ID, CODE, STEPRANGE, N, Dg, Ig, kg, α95g, Ds, Is, ks, α95s, comment,
JC24B-1, DirOPCA, M010-M030, 3, 243.3, 70.2, 0, 0.8, 243.3, 70.2, 0, 0.8, ""
JC24B-2, DirOPCA, M020-M040, 3, 245.1, 67.6, 0, 0.3, 245.1, 67.6, 0, 0.3, ""
JC24B-3, DirOPCA, M030-M040, 2, 246.2, 65.2, 0, 0.2, 246.2, 65.2, 0, 0.2, ""
JC24B, Fisher, site avg, 3, 245.0, 67.7, 1001.9,3.9, 245.0, 67.7, 1001.9,3.9, ""

JC

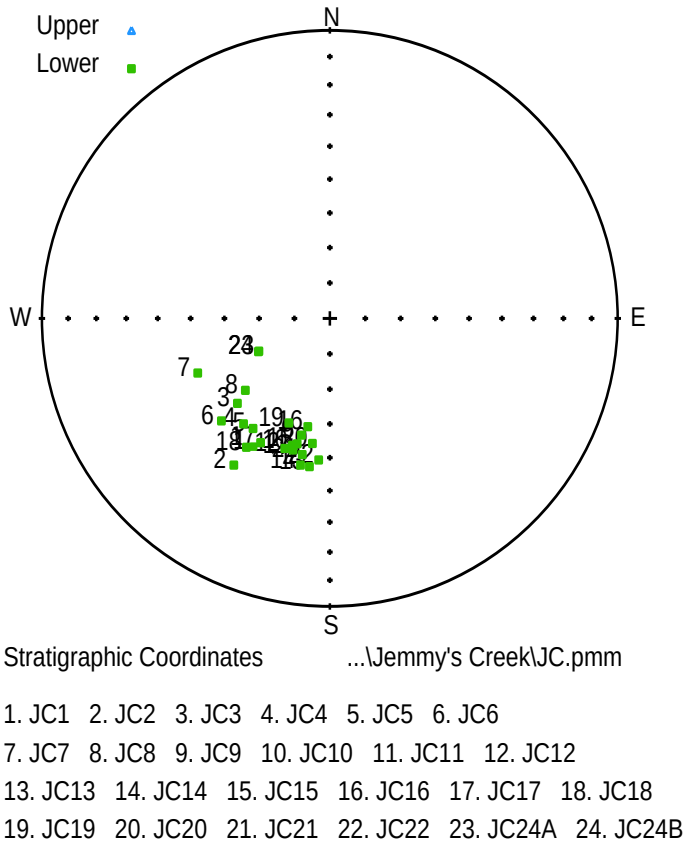

Figure 47: Declinations and inclinations without error circles of all flows (- JC23).

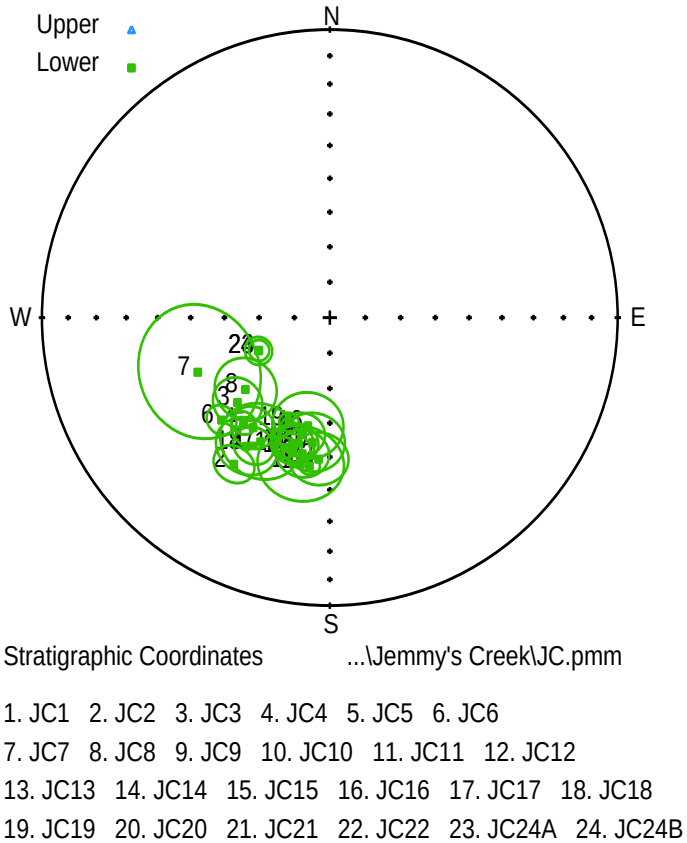

Figure 48: Final NMR directions for all 24 flows (except JC23 explained earlier) with error circles.

ID	CODE	STEPRANGE	N	Dec	Inc	α95
JC1	Fisher	site avg	3	210.8	47	5.5
JC2	Fisher	site avg	3	213.2	39	5.5
JC3	Fisher	site avg	3	227.4	54.1	7
JC4	Fisher	site avg	3	219.3	50.9	3.3
JC5	Fisher	site avg	3	214.9	51.5	6.1
JC6	Fisher	site avg	3	226.6	47	4.2
JC7	Fisher	site avg	3	247.5	48.9	18.1
JC8	Fisher	site avg	3	229.6	58.4	8.8
JC9	Fisher	site avg	3	193.6	55.7	6.3
JC10	Fisher	site avg	3	196.4	52.1	5.9
JC11	Fisher	site avg	3	195.6	50.8	4.6
JC12	Fisher	site avg	4	199.1	50.5	3.1
JC13	Fisher	site avg	3	187.8	46.9	2.7
JC14	Fisher	site avg	3	191.3	46.9	11.4
JC15	Fisher	site avg	3	194.6	52.9	5.7
JC16	Fisher	site avg	3	191.5	58.5	9.7
JC17	Fisher	site avg	3	209.1	49.1	11.1
JC18	Fisher	site avg	3	212.9	45.7	8.4
JC19	Fisher	site avg	3	201.4	58	2.7
JC20	Fisher	site avg	3	187.9	53.9	8.7
JC21	Fisher	site avg	3	191.4	50.1	7.1
JC22	Fisher	site avg	3	184.5	49.2	7.9
JC24A/B	Fisher	site avg	3	245.2	67.9	2.9

Table 1: Final NMR data for Jemmy's Creek (where N here is the number of samples used for the Fisher mean).

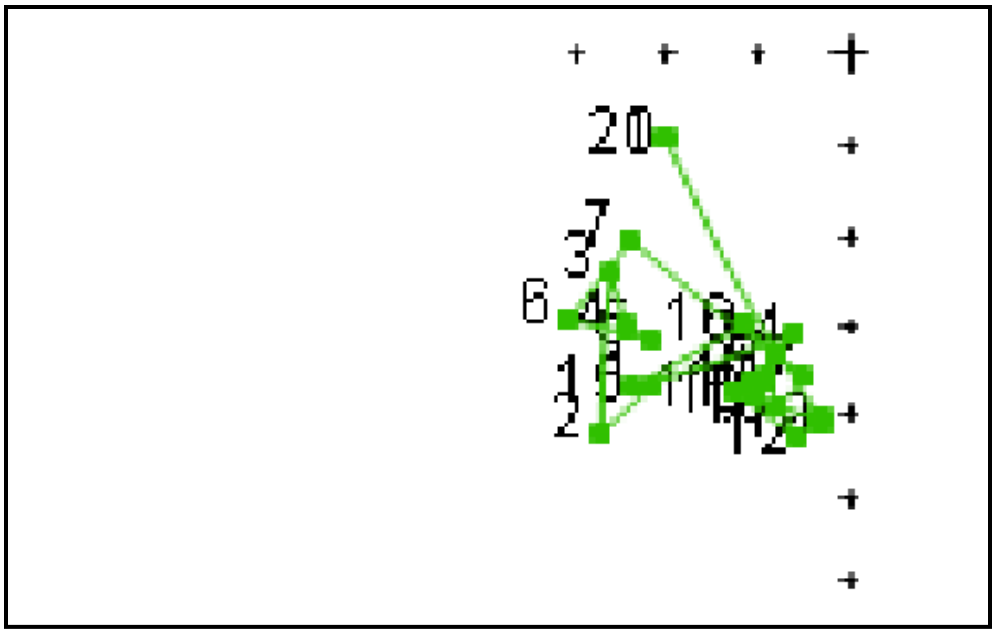

Figure 49: This is an up close look of final NMR directions, connecting consecutive flows while leaving out JC7, JC14, JC 17, and JC 23 due to error circles greater than or equal to α95's of 10.

VGP Results from our True Basic program		
Flow	vLat	vLong
1	-58.21	29.45
2	-51.99	26.00
3	-52.53	55.11
4	-55.68	43.62
5	-58.76	39.56
6	-48.77	46.79
7	-36.44	65.38
8	-53.74	62.86
9	-73.32	11.85
10	-69.10	12.26
11	-68.39	9.00
12	-66.65	15.40
13	-67.61	348.81
14	-66.75	356.47
15	-70.51	9.58
16	-76.71	12.73
17	-60.54	29.43
18	-56.21	30.87
19	-71.21	32.68
20	-73.67	354.28
21	-69.32	359.21
22	-70.09	342.00
24	-49.73	88.20

Table 2: Final VGP results assuming Jemmy's Creek was at Lat = 49.7° S, Long = 150.5° E approximately 40Ma.

Butler [5] not only gives equations for calculating the VGP positions, but also gives equations for the uncertainties.

$$dp = \frac{(1+3\,cos^2 p)}{2} \qquad \text{eqn 1}$$

$$dm = \alpha 95 \frac{\sin p}{\cos I_m} \qquad \text{eqn 2}$$

Where p is the magnetic colatitude from site to VGP and I_m is the sample's magnetic inclination. Equations 1 and 2 are set as the semi-minor and semi-major axes' respectively of an elliptical error plotted onto a VGP map projection.

Results and Conclusion

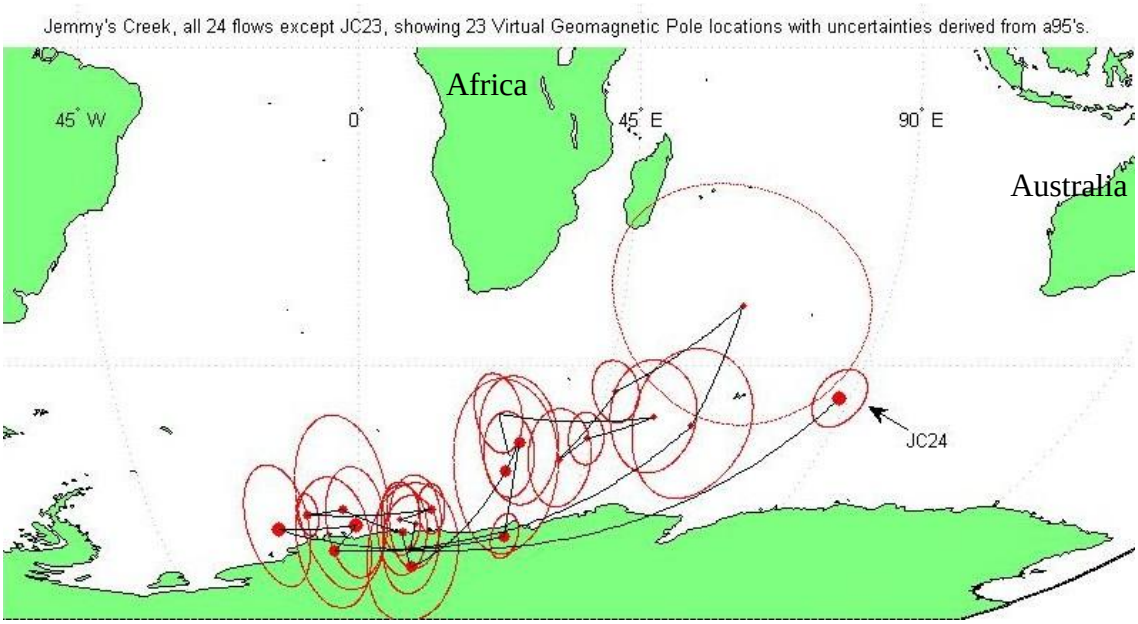

Figure 50: VGP's plotted with a new MATLAB program made by Joseph Dierkhising and me showing great circle paths and error ellipses.

The VGP locations start a bit high and drift towards Australia but after JC 8 they localize off of the cost of Antarctica. All VGP's show a reversed field for all 24 flows ~40 Ma.

The VGP path implies the reversed dipole field may have began slightly weaker than we see today for the first 8 flows (JC 1 through JC 8). Then, the path moves and stays off of the coast of Antarctica for flows JC9 through JC 22. For JC 23, there is chaotic behavior that could mean the dipole field was changing in some way during the time flow JC 23 was cooling. After JC 23, the VGP path travels towards Australia where VGP's have been found to reside when the dipole field dies out [7]. The Earth's magnetic field measured, minus the dipole filed, is typically called the non axial dipole (NAD) field.

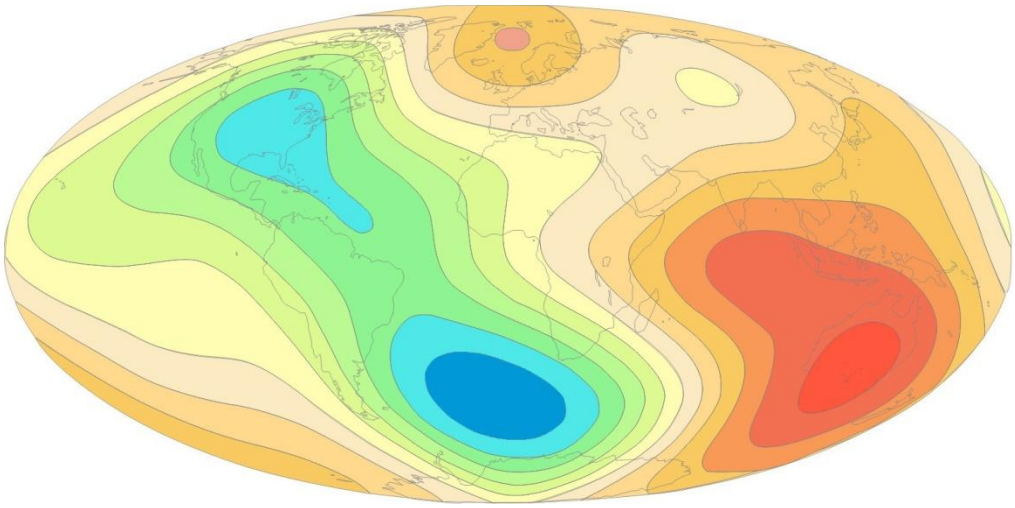

Figure 51: The Earth's NAD field averaged over the last 400 years.

There was a known flux patch off of the present west coast of Australia 40 Ma. Today, that patch has moved very little. My results show some of the VGP's are being influenced by this patch seen in red (figure 51). It would have been advantageous to sample even more flows past JC 24 but we were restricted from doing so geographically. It will be very interesting to know what amount of time has passed between each flow from JC1 to JC 24. Currently, I am working under Prof. Hoffman and he works with other professors around the world under NSF grants. One of the professors, Bradley S. Singer, Professor of Geochronology and Igneous Geochemistry at UW-Madison, dates the age of ancient volcanic cores using $^{40}Ar/^{39}Ar$ isotope dating. His findings will help to better understand how the Earth's geo-dynamo changes over time. Another collaborator, Pierre Camps from the University of Montpellier in France, analyzes the paleo-intensities, that is, the magnitudes of **m** within the cores.

Flow JC 24 shows promise of being consistent with a model that whenever the Earth's dipole field drops out the VGP's keep going towards the same location off of the western coast of Australia. A model that suggests there are two aspects to the Earth's magnetic field independent of each other but influenced by each other none the less. The results found agree with the fact that the NAD field has a large flux patch off the Australian coast. Therefore, going by this model, my results show a slight weakening of a reversed dipole field that then became fully reversed, and finally weakened once more (JC24) but never completely dropped off. If it did we would see VGP's appear closer to the western Australian coast.

References

[1] San Diego State University, 2004, http://sdsu-physics.org/NaturalScience100/Topics/2Earth/timages_earth/mag_revers2.gif

[2] Singer, B.S., Hoffman, K.A. et al., Structural and temporal requirements for geomagnetic field reversal deduced from $^{40}Ar/^{39}Ar$ dated lava flows, Nature, 434, 633-636 (2005).

[3] http://www.oceanleadership.org/wp-content/uploads/2009/07/81-300x219.jpg

[4] http://mail.colonial.net/~hkaiter/Aaa_web_images2012/4_1_5_0_magnetic_02.jpg

[5] Robert F. Butler, "Paleomagnetism: Magnetic Domains to Geologic Terranes," http://www.geo.arizona.edu/Paleomag/book/chap02.pdf, 1992

[6] http://bluegumpictures.com.au/images/medium/05/05_17772_75c.jpg

[7] Kenneth Hoffman, Pierre Camps, Gregory Fanjat, Mireille Perrin, Thierry Poidras, "AUSTRALASIAN VOLCANIC RECORDS OF THE EARTH'S MAGNETIC FIELD DURING POLARITY TRANSITIONS," http://www.ig.cas.cz/Castle2010/Abstracts/Camps.pdf, 2010.